

Use of Alkylarsonium Directing Agents for the Synthesis and Study of Zeolites

Dr. Sara Sáez-Ferre, Dr. Christian W. Lopes, Jorge Simancas, Dr. Alejandro Vidal-Moya, Dr. Teresa Blasco, Dr. Giovanni Agostini, Dr. Guillermo Mínguez Espallargas, Dr. Jose L. Jordá, Dr. Fernando Rey, Dr. Pascual Oña-Burgos

Abstract

Expanding the previously known family of -onium (ammonium, phosphonium, and sulfonium) organic structure-directing agents (OSDAs) for the synthesis of zeolite MFI, a new member, the arsonium cation, is used for the first time. The new group of tetraalkylarsonium cations has allowed the synthesis of the zeolite ZSM-5 with several different chemical compositions, opening a route for the synthesis of zeolites with a new series of OSDA. Moreover, the use of As replacing N in the OSDA allows the introduction of probe atoms that facilitate the study of these molecules by powder X-ray diffraction (PXRD), solid-state nuclear magnetic resonance (MAS NMR), and X-ray absorption spectroscopy (XAS). Finally, the influence of trivalent elements such as B, Al, or Ga isomorphically replacing Si atoms in the framework structure and its interaction with the As species has been studied. The suitability of the tetraalkylarsonium cation for carrying out the crystallization of zeolites is demonstrated along with the benefit of the presence of As atoms in the occluded OSDA, which allows its advanced characterization as well as the study of its evolution during OSDA removal by thermal treatments.

Introduction

Zeolites are crystalline microporous materials, mainly constituted by silicon oxide where the Si atom can be isomorphically replaced by other elements such as Al, B, Ga, Ti, Ge, or Sn. The well-defined size and distribution of the structural channels of each different zeolitic framework type together with the chemical composition confer to these materials multiple applications in processes such as gas adsorption and separation, catalysis, and encapsulation or controlled release of molecules, among others, some of them with industrial applications. **(1-9)** This is the driving force for studying novel methods for the preparation of new zeolitic structures, as it would give the possibility of obtaining tailored materials with the most appropriate channel system for each specific application. To date, up to 234 fully ordered as well as 11 partially disordered different zeolitic structures have been accepted by the International Zeolite Association, **(10)** and this number is constantly increasing.

Organic structure-directing agents (OSDAs) are fundamental tools for the preparation of zeolitic structures, **(11-13)** but their interaction with the zeolitic frameworks is unclear owing to the difficulty in localizing them in the crystalline structure. This is currently a challenge that usually requires the use of synchrotron radiation or characterization through single-crystal X-ray diffraction, which is very uncommon for zeolites. **(14-16)** Therefore, the development of straightforward and accessible methodologies to allow

the structural elucidation by using laboratory X-ray powder diffraction techniques is of clear interest.

In this sense, the incorporation of heavy atoms with high electron densities and large scattering factors could be of interest for the location of OSDA moieties placed inside of zeolite voids owing to the introduction of large electronic contrast. Phosphorous-containing OSDAs have been used for directing the crystallization of a number of zeolites, where N atoms of tetraalkylammonium OSDAs were substituted by P atoms, yielding tetraalkylphosphonium analogues. (17-23) This approach has produced a series of new zeolites, and the occluded organic cations were characterized by ^{31}P magic angle spinning (MAS) NMR spectroscopy. Additionally, the use of sulfonium compounds has also proved to be successful for the synthesis of some zeolitic materials. (24, 25) However, the electron density of the P or S atoms was insufficient for easily locating the organic template using lab data.

To date, the development of new OSDAs, based almost exclusively on ammonium, phosphonium, or even sulfonium cations, has enabled the synthesis of new zeolite structures. (26) Herein, we describe the use of a new family of OSDAs, tetraalkylarsonium cations, for the synthesis of the zeolite ZSM-5 (IZA code MFI), which is a proof of concept of the ability of arsonium cations as OSDAs for the synthesis of zeolites. Furthermore, we show that the use of arsenic plays an essential role in the study of the OSDA entrapped in the zeolite, as its higher electronic density with respect to phosphorus, sulfur, or nitrogen allows its facile localization by laboratory powder X-ray diffraction, as well as allows the use of ^{75}As MAS NMR and X-ray absorption spectroscopy (XAS) at the As K-edge to analyze the location and properties of the molecule. In this sense, the As atom can be considered as a probe inside the OSDA molecule to enable its study. Additionally, the removal of the OSDA by calcination and/or reduction has been also studied.

Results and Discussion

For this work, three tetraalkylarsonium cations have been synthesized: triethylmethylarsonium (OSDA-1), tetraethylarsonium (OSDA-2), and 1,4-bis-(triethylarsonium)butane (OSDA-3) cations as described in Scheme S1 (in the Supporting Information). The synthesis and characterization of all these cations is described in the Supporting Information. Moreover, safe handling is required to work with the triethylarsine precursor in the synthesis of arsonium cations and volatile arsenic-containing compounds formed during OSDA removal by thermal treatment, which is described in detail in the Supporting Information. At this point, it should be indicated that arsonium cations themselves are really stable and have low toxicity. (27)

Zeolite MFI was obtained as a single phase when using OSDA-2 as described in the Supporting Information (Figures S11 and S12). The samples show the typical coffin shape of MFI materials observed for high silica materials (Figures S21–S24 in the Supporting Information). (28) This result is consistent with the observed crystallization of zeolite MFI when using the analogous tetraethylammonium and tetraethylphosphonium cations as OSDAs.

Interestingly, OSDA-1 and OSDA-3 gave similar results, although longer crystallization times were required (typically 21 days), suggesting that the common triethylarsonium moiety is driving the crystallization to the MFI zeolitic material.

Moreover, replacing part of the silica source with GeO_2 , Al_2O_3 , $\text{Ga}(\text{NO}_3)_3$, or H_3BO_3 in the crystallization media allows the isomorphic incorporation of those elements into the zeolitic framework when OSDA-2 is used as the structure-directing agent (Figures S11 and S12 in the Supporting Information). However, this substitution does not occur when either of the other two OSDAs were used and only amorphous solids were recovered under similar conditions, which was pure silica MFI (Figure S11 b in the Supporting Information).

After performing the synthesis, the structural integrity of the OSDA inside the pure as-made silica zeolite was checked. Chemical analyses of the as-made sample revealed a C/As ratio equal to 8, very close to theoretical value of the OSDA-2 (Table S2 in the Supporting Information). Also, the chemical shift of the signal appearing at 250 ppm in the ^{75}As MAS NMR spectrum of the OSDA-2-containing zeolite Si-MFI is almost identical to that of the free OSDA (Figure 1). The larger broadening for the OSDA-2@MFI material can be associated to an increase of the quadrupole coupling constant of the ^{75}As ($I = 3/2$). The confinement of the OSDA-2 within the zeolite channels decreases the mobility of the cation and enhances the electric field gradients of its surrounding. In addition, the integrity of the OSDA under the synthesis conditions was carefully studied by ^1H NMR spectroscopy. In this sense, the ^1H NMR spectrum was acquired for the mother liquor and compared with the ^1H NMR spectrum for the free OSDA in solution (Figure S14 in the Supporting Information). Comparison of both spectra confirms again that the OSDA is stable under the synthesis conditions. As the OSDA-2 remains unchanged after MFI crystallization, its exact location inside of the zeolite structure was obtained with only lab X-ray data. In order to do so, the orthorhombic structure of MFI of the as-made material obtained by using tetrapropylammonium as the OSDA, (29) excluding the organic component, was used as the starting point. Then, a difference Fourier map was calculated by using the programs FullProf and GFourier. This map allowed easy determination of the location of the arsenic atoms, owing to their high electron density, which reveals the otherwise elusive position of the molecule. Moreover, the approximated locations of the four C atoms connected to As (Figure 2 top and Figure S13 in the Supporting Information) have also been easily obtained. The four remaining C atoms were located close to the previous ones, and geometrical restraints were imposed prior to the refinement. The used restraints were obtained from the single-crystal X-ray diffraction analysis of the pure OSDA (Figure S10 and Table S1 in the Supporting Information). Lastly, a fluorine ion was placed close to the 4 ring, as it has been widely described that F^- species are located close to those units. (30) The lab PXRD pattern was refined by using the program FullProf, obtaining good residual values, as well as a good match between the experimental and calculated patterns (Figure 2 bottom).

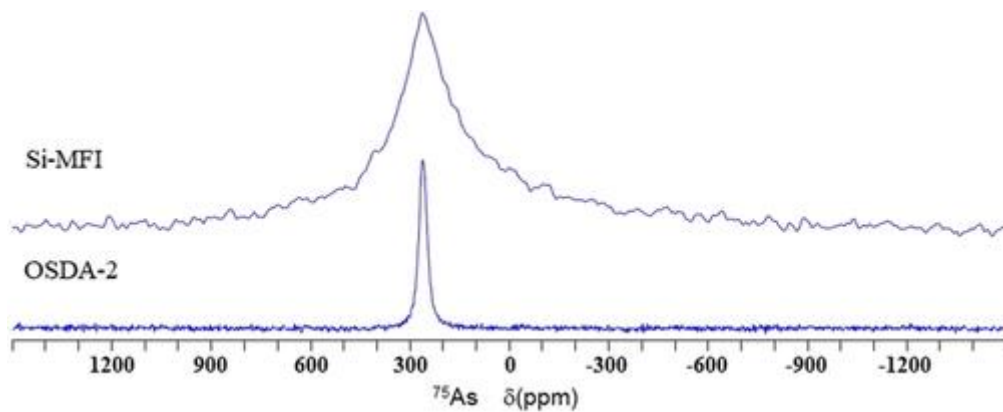


Figure 1

^{75}As MAS NMR spectra for a) the OSDA-2 and b) as-prepared Si-MFI.

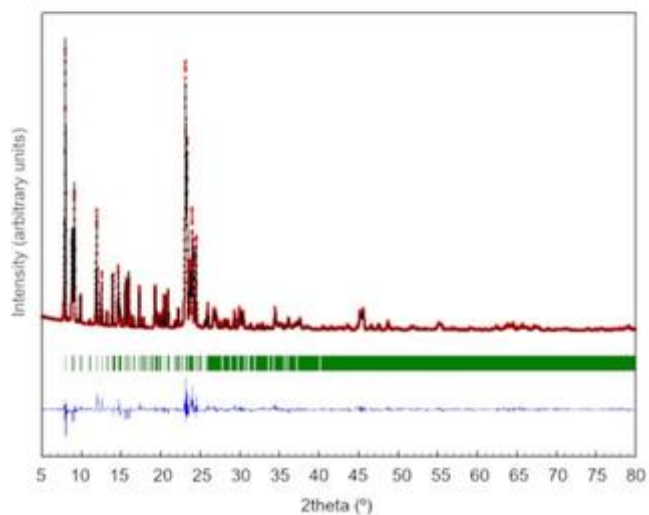
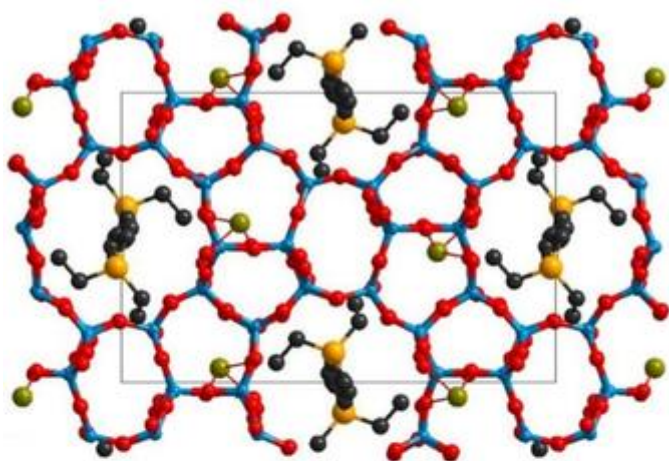


Figure 2

Top: OSDA-2 localized inside the zeolite Si-MFI (Si=blue, O=red, As=gold, C=black, and F=green). Bottom: Rietveld refinement of the X-ray diffraction pattern of as-made MFI. Observed (red circles) and calculated (black line) XRPD patterns, and the corresponding

difference profile (bottom, blue line). The green short tick marks below the pattern give the positions of the Bragg reflections. Residual values ($R_{wp}=14.1$, $R_{exp}=2.36$, $R_B=7.70$, $R_F=5.26$).

One interesting fact is that the location of the OSDA-2 in MFI is very similar for both tetraethylarsonium, herein determined by lab PXRD, and tetrapropylammonium, previously found by single-crystal X-ray diffraction. (29) Therefore, both organic cations, based on arsenic and nitrogen atoms, respectively, seem to have an analogous interaction with the zeolitic framework. In addition, the location of F^- is in good agreement with that suggested by using ^{19}F MAS NMR data (Figure S15 in the Supporting Information), where a main F NMR signal was observed at -67 ppm. (30)

Further analysis of the as-made sample was done by X-ray absorption spectroscopy. In this sense, we must take into account that, although alkylammonium, and less frequently phosphonium cations, are by far the most commonly used molecules as OSDAs, the X-ray absorption edges of N or P atoms are at very low energies and their XAS spectra cannot be easily measured. Distinctly here, we can profit from the presence of a heavy atom in the OSDA-2 cation and perform its characterization by XAS at the As K-edge (11 867 eV). So, the organic cation containing As, either in its iodide form or entrapped inside the MFI channels after hydrothermal zeolite synthesis, was investigated by XAS, allowing us to further probe the stability of the As species during the hydrothermal synthesis.

The X-ray absorption near edge structure (XANES) region of the OSDA-2 in its iodide form and those entrapped inside of the zeolite channels are nearly identical (Figure 3 a), indicating that the As-containing OSDA remains intact inside all the zeolites obtained in this study, in good agreement with the ^{75}As NMR (Figure 1) and chemical analyses (Table S2 in the Supporting Information). The fitting of the extended X-ray absorption fine structure (EXAFS) data of the pure OSDA-2 with As-C contribution gives a coordination number around four (Figure 3 b and Table 1); also very close to that obtained for the EXAFS spectrum of the as-synthesized material, with distances of 1.932 ± 0.005 Å. This is in good agreement with the theoretical and also crystallographic structure of the $[OSDA-2]^+I^-$ salt, solved by single-crystal XRD. The as-made zeolites show similar edge positions and features beyond the edge of the OSDA-2, which confirms that organic template species are stable during the zeolite syntheses. At this point, the OSDAs entrapped in the MFI materials containing different heteroatoms (B, Al, Ga, and Ge) were also studied by means of XAS. The corresponding XANES and EXAFS spectra are shown in Figure 3 and fitted EXAFS parameters are reported in Table 1.

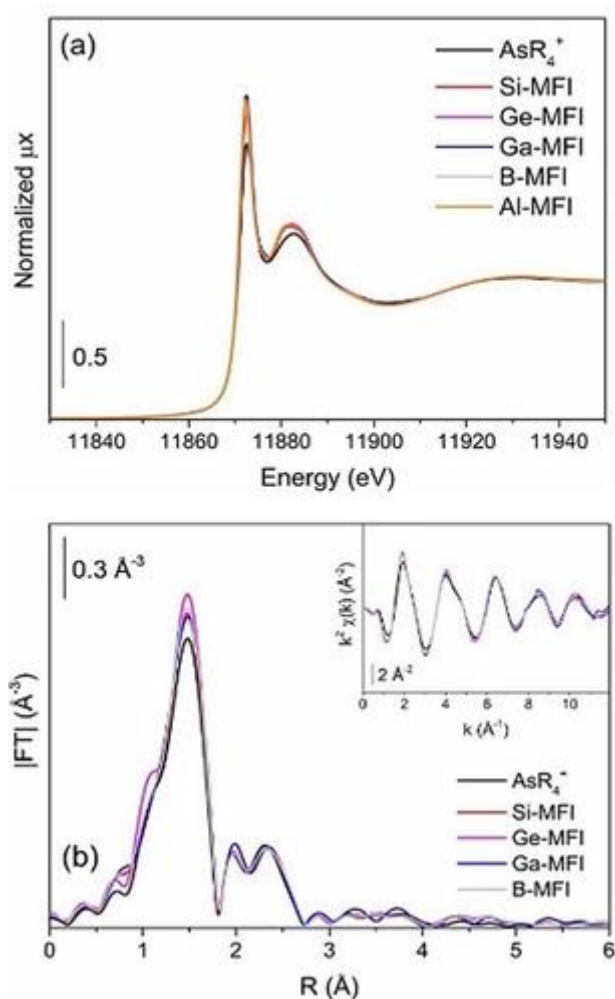


Figure 3

a) Normalized XANES spectra at the As K-edge and b) |FT| of k^2 -weighted $\chi(k)$ functions of crystallized AsR₄⁺ and as-synthesized As@zeolites MFI. Inset of b) represents the k^2 -weighted $\chi(k)$ functions of the displayed data.

Table 1. Summary of optimized parameters by fitting EXAFS data of crystallized AsR₄⁺ and as-synthesized As@MFI materials.^[a]

Sample	N_{As-C}	R_{As-C} [Å]	σ^2 [Å ²]	ΔE_0 [eV]	R factor
OSDA-2	4.0±0.2	1.932±0.005	0.0018±0.0004	7.7±0.3	0.00877
Si-MFI	4.5±0.2	1.936±0.004			0.00653
Ge-MFI	4.8±0.2	1.937±0.004			0.00909
Ga-MFI	4.5±0.4	1.938±0.009			0.01567

Sample	$N_{\text{As-C}}$	$R_{\text{As-C}} [\text{\AA}]$	$\sigma^2 [\text{\AA}^2]$	$\Delta E_0 [\text{eV}]$	R factor
B-MFI	4.5±0.2	1.940±0.003			0.00634

[a] A simultaneous fit of the spectra was adopted, fixing the σ^2 and ΔE_0 values; the fits were performed on the first coordination shell ($\Delta R=1.0-2.0 \text{\AA}$) over FT of the $k_1k_2k_3$ -weighted $\chi(k)$ functions performed in the $\Delta k=2.0-12.0 \text{\AA}^{-1}$ interval, resulting in a number of independent parameters of $2\Delta R\Delta k/\pi=31.0$. $S_0^2=0.86$.

The MFI materials were calcined under dry air at 650 °C, observing by XRD that all of them are stable after calcination (Figure S27 in the Supporting Information). However, there are clear differences in the final As content in the calcined materials depending on the presence of trivalent heteroatoms isomorphically incorporated into the MFI framework. Indeed, after calcination, no As is observed in the samples containing only tetravalent (i.e., Si and Ge) atoms. Whereas around 50 % of the initial As content is still present after calcination for those MFI zeolites containing trivalent elements like Ga, Al, or B. In these cases, the molar ratio of trivalent element to As (M/As) is close to 1 (see Table S3 in the Supporting Information). These results strongly suggest that the arsenic atoms that are not interacting with the trivalent element evolve out of the zeolite during calcination, whereas the arsenic that interacts with the T^{III} elements is retained inside the zeolite. Thus, the presence of trivalent elements plays a pivotal role to keep the arsenic inside the porous network of the zeolite. However, the ^{75}As MAS NMR spectra of the calcined samples do not show any resonance, despite the as-made materials giving the broad bands characteristic of the OSDA inside the zeolite (Figure S28 in the Supporting Information) and chemical analyses indicate that a significant amount of As remains within the zeolite upon calcination. The absence of As signals is due to the formation of low-symmetry species with very large quadrupole couplings giving broad signals that become undetectable by conventional NMR experiments. (31)

When the as-made sample is treated under hydrogen at high temperature instead of by calcination (Figure S27 in the Supporting Information), As atoms are removed independently of the chemical composition of the framework (see Table S3 in the Supporting Information).

Additionally, the isomorphous incorporation of the trivalent Al and Ga cations into the framework positions was further confirmed by ^{27}Al and ^{71}Ga MAS NMR spectroscopy, respectively. The ^{27}Al MAS NMR spectra of the as-synthesized and calcined MFI samples are shown in the Supporting Information (Figure S29 in the Supporting Information). The ^{27}Al MAS NMR spectra of the as-made and calcined samples show a main signal centered at 52 ppm, which is assigned to aluminum in tetrahedral sites. (32) Also, a residual resonance is observed at 0 ppm, which is typically attributed to the presence of extra-framework aluminum in the zeolite. (32) For the Ga-containing material, resonances at 152 ppm in the ^{71}Ga MAS NMR spectra of the as-synthesized and calcined samples were detected (Figure S30 in the Supporting Information) and assigned to gallium in tetrahedral coordination, corresponding to framework positions. (33)

The evolution of the As species within MFI structure during calcination in air was “in situ” studied with the Ga-MFI sample. The raw data of the XANES region indicate that by increasing the temperature (Figure 4), the characteristic features present in the

spectrum of OSDA-2 are maintained until approximately 500 °C, where the oscillation centered at 11 882 eV starts to disappear, indicating that the local structure around the As atom was modified above this temperature as a consequence of the OSDA decomposition (in agreement with the thermogravimetric analysis (TGA) data shown in Figures S16–S20 in the Supporting Information).

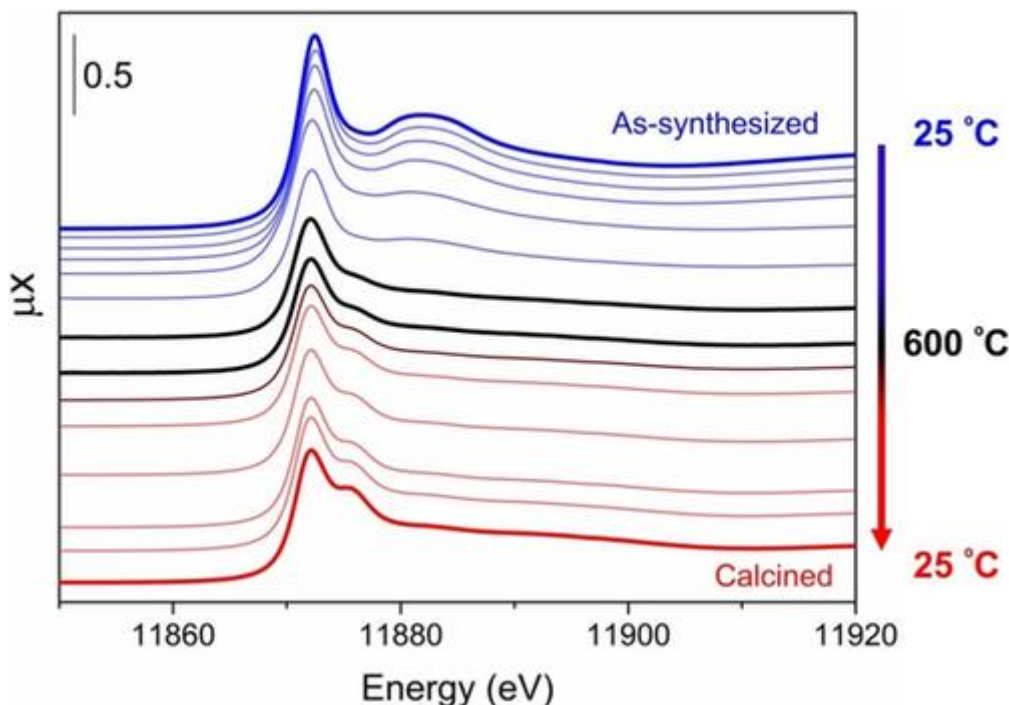


Figure 4

Raw XANES spectra at the As K-edge of Ga-MFI zeolite during calcination: the shoulder at 11 882 eV characteristic of the OSDA is lost through the thermal treatment.

When the temperature reaches 600 °C, this feature becomes flatter and a shoulder at 11 875 eV grows as the temperature decreases to 25 °C. This feature could be attributed to the oxidation of As^{3+} to As^{5+} , however, the edge position is maintained as that characteristic for As^{3+} . (34) Moreover, 33 % of As was released during calcination, most likely as volatile AsR_3 , which is formed during this thermal treatment (Table S4 in the Supporting Information). This value is in reasonable agreement with the chemical analysis of the Ga-MFI sample submitted to calcination in the laboratory. A similar behavior has been observed by our group for phosphorous-containing cations, which were transformed into phosphate-like species upon calcination. (23)

The XANES spectra of the As-Ga-MFI after thermal treatments under hydrogen at 600 °C exhibit a similar feature, but with some differences in terms of the amount of As released. When the fresh Ga-MFI sample is directly reduced in H_2 , only a small fraction of As remains ($\approx 5\%$ —Table S4 in the Supporting Information) at the end of the thermal treatments as the presence of H_2 facilitates the formation of volatile AsR_3 species. On the other hand, the subsequent reduction of the calcined As-Ga-MFI material shows that around 20 % of the As atoms is still present in the zeolite at the end of the subsequent reduction, demonstrating that the calcination treatment is able to stabilize most of the As atoms against reduction in the zeolite.

To investigate the different As species formed on Ga-MFI depending on the thermal treatment, the samples were “in situ” studied during calcination, reduction, and calcination-reduction treatments. The normalized XANES spectra of these samples are compared with those of standard As compounds in Figure 5 a. The XANES spectra for samples after any thermal treatment are rather similar regardless of the heating procedure or atmosphere employed, with same edge position (ca. 11 870 eV) as for OSDA-2, indicating that the formal oxidation state is maintained as As³⁺. However, as stated above, the oscillation at 11 882 eV present for OSDA-2 is lost upon any of the studied thermal treatments, demonstrating that the organic compound decomposes at the end of the experiments. Furthermore, the shape of the spectra does not resemble those of arsenic oxides (i.e., As₂O₃ and As₂O₅) or that for As⁰, indicating that different species are formed in the zeolites. However, the shape of the XANES spectra displayed here is compatible with those found for As³⁺ cations adsorbed on surfaces in experiments of wastewater remediation, consisting in arsenic inner(outer) complexes. (35-37) Aiming to obtain more detailed information on the local structure of these As-based species, the EXAFS region was analyzed (Figure 5 b). Only a first-shell As–O contribution is seen in most |FT| for thermally treated samples, pointing out that As atoms are involved in a highly dispersed or disordered arrangement. Furthermore, different intensities of As–O contribution can be observed, which indicates that As atoms are differently coordinated or display unlike static disorder (different Debye–Waller factors). To disentangle these questions, quantitative information was extracted by treating the EXAFS data, which is gathered in the Supporting Information (Table S5 and Figure S31 for fitted data). The three thermally treated samples show a coordination number around As of 3.5, with As–O distances of approximately 1.75 Å (within errors). These values are in agreement with those found in the literature for As bound to the surface of adsorbents (inner-shell complexes). (35-38) However, the samples that underwent the calcination process (calcined and calcined-reduced) show similar Debye–Waller factors, whereas the reduced one showed a significantly higher value, suggesting that As atoms are in a more disordered local environment, which can explain its lower As–O first-shell contribution intensity at |FT| with respect to those that have undergone a calcination process. The meaningful ΔE_0 value is also in agreement with those found in the literature for As-based species studied by XAS. (38, 39)

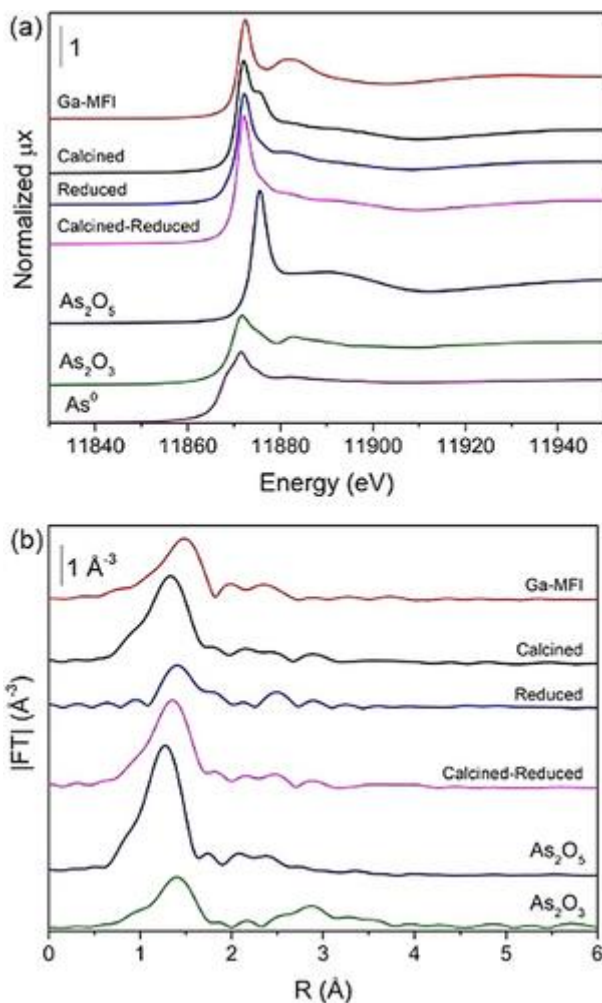


Figure 5

a) Normalized XANES spectra at the As K-edge and b) $|FT|$ of k^2 -weighted $\chi(k)$ functions of Ga-MFI before and after thermal treatments and As-based standards.

Finally, the nature of the Ga species present in the zeolitic framework was also studied by XAS at the Ga K-edge. The XANES spectrum of the as-synthesized Ga-MFI (Figures S32 and S33 in the Supporting Information) is similar to that reported for Ga-substituted zeolite Beta, (40) with the absorption edge positioned at 10 372 eV, typical of Ga^{3+} . Moreover, no indication of the Ga_2O_3 phase can be observed in the XAS spectrum of the as-made material. By submitting the samples to the different thermal treatments (calcination, reduction, and calcination-reduction) the Ga atoms remain mostly tetrahedrally coordinated, with exception of the sample after calcination-reduction. In this case, a shoulder at 10 367 eV appeared, showing that a small portion of Ga atoms are reduced after subsequent calcination-reduction treatments, which can be interpreted as a migration of Ga from framework to extra-framework positions. Isolating the EXAFS region of the spectra gives rise to the presence of a predominant first-shell Ga-O contribution in the case of Ga-MFI before and after treatments, which is rather different with respect to that of Ga_2O_3 (see the Supporting Information, Figure S32 and Table S6 for fitted data). A decrease in the intensity of this first-shell contribution is observed after thermal treatments, as previously reported. (41) The as-synthesized Ga-MFI still containing the OSDA-2 gives a coordination number of four with Ga-O distances of approximately 1.78 Å (within errors, see Table S6 in the Supporting Information), in

agreement with data reported in the literature. ([40](#), [42](#)) These results confirm that Ga atoms are tetrahedrally coordinated within the MFI framework in excellent agreement with previously discussed ^{71}Ga MAS NMR results.

Conclusion

This study has achieved several milestones, which could become a breakthrough in the synthesis of zeolites. First, we have demonstrated that alkylarsonium can be used as an efficient OSDA for the synthesis of zeolite MFI. This achievement could open the possibility for obtaining novel zeolites as previously occurred with phosphonium organocations with respect to N-based OSDAs. ([17-23](#)) Also, we have shown that arsenic atoms included in OSDAs can be used as useful probe moieties to understand the behavior of organic structure-directing agents during the thermal treatments for zeolite activation. The high electron density of arsenic atoms is extremely helpful to localize the OSDA in the zeolitic structure by powder X-ray diffraction, and the location of the OSDA molecule in the MFI structure is analogous to that described for the ammonium derivate. Additionally, the presence of As in the OSDA allows the study of the OSDA and of the As species trapped in the zeolite after calcination by ^{75}As MAS NMR spectroscopy and XAS at the As K-edge. Finally, it has been shown that arseniate-like species interact with the trivalent Ga sites at the framework during the thermal treatments of the samples. Then, we have shown that arsenic atoms are useful for characterization and evolution of OSDA entrapped in the zeolitic voids.

Experimental Section

Detailed information on the conditions for sample preparation and of data acquisition and analysis for the different techniques are provided in the Supporting Information.

Data availability

CCDC 1910863 contains the supplementary crystallographic data for this paper. These data are provided free of charge by The Cambridge Crystallographic Data Centre.

All other data supporting the results are available within the article and its Supporting Information, or from the corresponding authors upon reasonable request.

Acknowledgements

Program Severo Ochoa SEV-2016-0683 and Maria de Maeztu MDM-2015-0538 are gratefully acknowledged. S.S-F. thanks MEC for his Severo Ochoa Grant SPV-2013-067884, P.O.-B. and G.M.E. thank MEC for his Ramón y Cajal contracts (RYC-2014-16620 and RYC-2013-14386). The authors thank the financial support by the Spanish Government (RTI2018-096399-A-I00, RTI2018-101784-B-I00 and CTQ2017-89528-P) and the Generalitat Valenciana (PROMETEO/2017/066). The Electron Microscopy Service of the UPV is acknowledged for their help in sample characterization. We gratefully acknowledge ESRF synchrotron for allocating beamtime (proposal CH-5193), the Italian CRG beam-line at ESRF (LISA-BM08), and Alessandro Puri for the help and

technical support during our experiment. C.W.L. (Science without Frontiers—Process no. 13191/13-6) thanks CAPES for a predoctoral fellowship.

Conflict of interest

The authors declare no conflict of interest.

References

1. J. Sun, C. Bonneau, A. Cantin, A. Corma, M. J. Diaz-Cabañas, M. Moliner, D. Zhang, M. Li, X. Zou, *Nature* 2009, **458**, 1154– 1157.
2. J. Jiang, J. Yu, A. Corma, *Angew. Chem. Int. Ed.* 2010, **49**, 3120– 3145; *Angew. Chem.* 2010, **122**, 3186– 3212.
3. A. Corma, *J. Catal.* 2003, **216**, 298– 312.
4. M. E. Davis, *Nature* 2002, **417**, 813– 821.
5. R. M. Shayib, N. C. George, R. Seshadri, A. W. Burton, L. S. I. Zones, B. F. Chmelka, *J. Am. Chem. Soc.* 2011, **133**, 18728– 18741.
6. Z. Wang, J. Yu, R. Xu, *Chem. Soc. Rev.* 2012, **41**, 1729– 1749.
7. A. Corma, M. E. Davis, *ChemPhysChem* 2004, **5**, 304– 313.
8. S. I. Zones, *Microporous Mesoporous Mater.* 2011, **144**, 1– 8.
9. G. Bellussi, A. Carati, R. Millini, in *Zeolites and Catalysis: Synthesis Reactions and Applications, Vol. 2* (Eds.:), Wiley-VCH, Weinheim, 2010, p. 449.
10. International Zeolite Association Website, <http://www.iza-online.org/> (accessed October 4, **2018**).
11. A. W. Burton, S. I. Zones, *Stud. Surf. Sci. Catal.* 2007, **168**, 137– 179.
12. A. W. Burton, S. I. Zones, S. Elomari, *Curr. Opin. Colloid Interface Sci.* 2005, **10**, 211– 219.
13. S. I. Zones, Y. Nakagawa, G. S. Lee, C. Y. Chen, L. T. Yuen, *Microporous Mesoporous Mater.* 1998, **21**, 199– 211.
14. A. B. Pinar, L. B. McCusker, C. Baerlocher, S.-J. Hwang, D. Xie, A. I. Benin, S. I. Zones, *New J. Chem.* 2016, **40**, 4160– 4166.
15. S. Smeets, L. B. McCusker, C. Baerlocher, S. Elomari, D. Xie, S. I. Zones, *J. Am. Chem. Soc.* 2016, **138**, 7099– 7106.
16. S. Smeets, L. B. McCusker, C. Baerlocher, D. Xie, C.-Y. Chen, S. I. Zones, *J. Am. Chem. Soc.* 2015, **137**, 2015– 2020.
17. D. L. Dorset, G. J. Kennedy, K. G. Strohmaier, M. J. Diaz-Cabanás, F. Rey, A. Corma, *J. Am. Chem. Soc.* 2006, **128**, 8862– 8867.

18. A. Corma, M. J. Diaz-Cabanas, J. L. Jorda, F. Rey, G. Sastre, K. G. Strohmaier, *J. Am. Chem. Soc.* 2008, **130**, 16482– 16483.
19. A. Corma, M. J. Díaz-Cabañas, J. Jiang, M. Afeworki, D. L. Dorset, S. L. Soled, K. G. Strohmaier, *Proc. Natl. Acad. Sci. USA* 2010, **107**, 13997– 14002.
20. D. L. Dorset, K. G. Strohmaier, C. E. Kliewer, A. Corma, M. J. Díaz-Cabañas, F. Rey, C. J. Gilmore, *Chem. Mater.* 2008, **20**, 5325– 5331.
21. R. Simancas, D. Dari, N. Velamazán, M. T. Navarro, A. Cantin, J. L. Jorda, G. Sastre, A. Corma, F. Rey, *Science* 2010, **330**, 1219– 1222.
22. M. Hernández-Rodríguez, J. L. Jorda, F. Rey, A. Corma, *J. Am. Chem. Soc.* 2012, **134**, 13232– 13235.
23. J. Simancas, R. Simancas, P. J. Bereciartua, J. L. Jorda, F. Rey, A. Corma, S. Nicolopoulos, P. Pratim-Das, M. Gemmi, E. Mugnaioli, *J. Am. Chem. Soc.* 2016, **138**, 10116– 10119.
24. C. Jo, S. Lee, S. J. Cho, R. Ryoo, *Angew. Chem. Int. Ed.* 2015, **54**, 12805– 12808; *Angew. Chem.* 2015, **127**, 12996– 12999.
25. S. Lee, C. Jo, H. Park, J. Kim, R. Ryoo, *Microporous Mesoporous Mater.* 2019, **280**, 75– 81.
26. F. Rey, J. Simancas, *Beyond Nitrogen OSDAs in Insights into the Chemistry of Organic Structure-Directing Agents in the Synthesis of Zeolitic Materials* (Ed.), Springer, Cham, 2018, pp. 103– 138.
27. D. Fattorini, A. Notti, F. Regoli, *Chem. Ecol.* 2006, **22**, 405– 414.
28. G. Bonilla, I. Díaz, M. Tsapatsis, H. K. Jeong, Y. Lee, D. G. Vlachos, *Chem. Mater.* 2004, **16**, 5697– 5705.
29. H. van Koningsveld, H. van Bekkum, J. C. Jansen, *Acta Crystallogr. Sect. B* 1987, **43**, 127– 132.
30. C. A. Fyfe, D. H. Brouwer, A. R. Lewis, J. M. Chézeau, *J. Am. Chem. Soc.* 2001, **123**, 6882– 6891.
31. G. Balimann, P. S. Pregosin, *J. Magn. Reson.* 1977, **26**, 283– 289.
32. J. Klinowski, *Chem. Rev.* 1991, **91**, 1459– 1479.
33. C. R. Bayense, J. H. C. van Hooff, A. P. M. Kentgens, J. W. de Haan, L. J. M. van de Ven, *J. Chem. Soc. Chem. Commun.* 1989, 1992– 1993.
34. J. Canche-Tello, M. C. Vargas, J. Hernandez-Cobos, I. Ortega-Blake, A. Leclercq, P. L. Solari, J. Lezama-Pacheco, C. Den Auwer, J. M. de Leon, *J. Phys. Chem. A* 2015, **119**, 2829– 2833.
35. Y. Arai, E. J. Elzinga, D. L. Sparks, *J. Colloid Interface Sci.* 2001, **235**, 80– 88.
36. M. L. Farquhar, J. M. Charnock, F. R. Livens, D. J. Vaughan, *Environ. Sci. Technol.* 2002, **36**, 1757– 1762.
37. G. Morin, G. Ona-Nguema, Y. Wang, N. Menguy, F. Juillot, O. Proux, F. Guyot, G. Calas, G. E. Brown, Jr., *Environ. Sci. Technol.* 2008, **42**, 2361– 2366.

38. A. Ramírez-Solís, R. Mukopadhyay, B. P. Rosen, T. L. Stemmler, *Inorg. Chem.* 2004, **43**, 2954– 2959.
39. J. Canche-Tello, M. C. Vargas, J. Hernandez-Cobos, I. Ortega-Blake, A. Leclercq, P. L. Solari, C. Den Auwer, J. Mustre de Leon, *J. Phys. Chem. A* 2014, **118**, 10967– 10973.
40. C. Prieto, T. Blasco, M. Cambor, J. Pérez-Pariente, *J. Mater. Chem.* 2000, **10**, 1383– 1387.
41. C. Lamberti, G. Turnes Palomino, S. Bordiga, A. Zecchina, G. Spanò, C. Otero Areán, *Catal. Lett.* 1999, **63**, 213– 216.
42. S. A. Axon, K. Huddersman, J. Klinowski, *Chem. Phys. Lett.* 1990, **172**, 398– 404.